Modal Actuation and Sensing With an Active AFM Cantilever

Mohammad Mahdavi, *Member, IEEE*, Hazhir Mahmoodi Nasrabadi, Mohammadreza Soleymaniha, and S. O. Reza Moheimani, *Fellow, IEEE*

***Abstract*—Modal actuation and sensing are implemented on a microfabricated AFM cantilever with a two-layer piezoelectric stack transducer. The top transducer is shaped as the second derivative of the first mode shape. The bottom transducer is uniformly distributed along the cantilever length. The purpose of this work is to demonstrate that modal actuation and sensing can be used to eliminate other resonances from frequency response function of the active cantilever, except the first mode. First-order mathematical formulations are presented to model transverse vibrations of the cantilevers under this study. Microfabrication steps and characterization of these cantilevers are reported. Their respective actuation and sensing gains are determined for comparison with conventional active cantilevers. Electromechanical coupling coefficients are also calculated to exhibit reciprocity of modal actuation and sensing in eliminating higher modes from the frequency response. The advantages of modal actuation and sensing in avoiding instabilities in feedback controlled AFM active cantilevers are also demonstrated.**

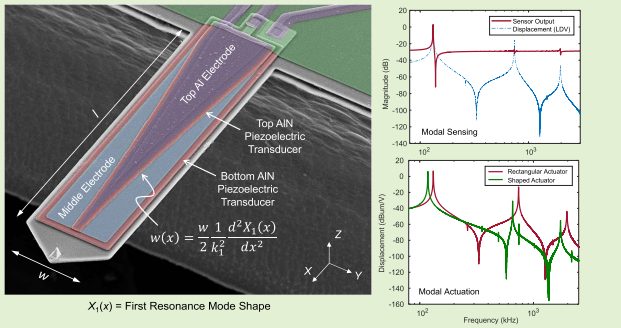

$X_1(x)$ = First Resonance Mode Shape

***Index Terms*— Active microcantilever, atomic force microscopy, microelectromechanical systems, microfabrication, modal actuation, modal sensing, piezoelectric devices.**

I. Introduction

RECENT advances in micromachining and microfabrication have led to emergence of new micro/nanoscale devices and scaling electromechanical devices down to microscales. Instances of such microelectromechanical systems (MEMS) are inertial sensors [1], nano-positioners [2], [3] and a wide variety of sensors and microsystems [4]–[6]. The microcantilever is a microscale flexible structure placed at the heart of an atomic force microscope (AFM). In an AFM setup, the cantilever tip interacts with a specimen, and measurements of cantilever deflection are used to reveal various properties of the surface, from topography to material/mechanical properties. Advances in microfabrication technology have enabled the fabrication of MEMS Si and SiN AFM microcantilevers that are used in many fields of science and technology.

There has been a consistent effort to integrate actuators and sensors on the AFM cantilevers in order to improve their performance and functionalities [7], [8]. A cantilever with such capabilities is used in dynamic atomic force microscopy, where the cantilever is excited to vibrate at its first resonance mode. The ability to collocate the sensor and actuator on the cantilever is among the most important advantages of the resulting devices. Collocation results in interlacing poles and zeros in the system's frequency response function (FRF) [9]. This enables the design and implementation of highly robust feedback control loops to manipulate the quality factor (Q) of the desired mode as needed [10].

Integration of sensors and actuators into flexible structures has been an active field of research for the past three decades. Patches of piezoelectric elements such as polyvinylidene fluoride (PVDF) or lead zirconate titanate (PZT) layers have been attached to a macroscale beam to excite the beam into vibration and sense its motion [9], [11]–[13]. Applying a wideband voltage across a uniformly distributed actuator can excite multiple resonance modes of the beam. When used in a closed-loop control system, unmodeled dynamics of the beam at higher frequencies can lead to instability. This phenomenon is known as the spillover effect [14]. This issue can be addressed by using control design methods such as positive position feedback control, resonant control and integral resonant control as long as the underlying structures are equipped with collocated and compatible sensors and actuators [9], [10], [15]. However, avoiding the spillover effect without perfect actuator/sensor collocation becomes challenging. Plus, extra electronics add further dynamics and noise to the

Manuscript received December 5, 2020; revised January 5, 2021; accepted January 14, 2021. Date of publication January 19, 2021; date of current version March 5, 2021. This work was supported by the U.S. Department of Energy's Office of Energy Efficiency and Renewable Energy (EERE) under Advanced Manufacturing Office Award under Grant DE-EE0008322. The associate editor coordinating the review of this article and approving it for publication was Prof. Sheng-Shian Li. *(Corresponding author: S. O. Reza Moheimani.)*

The authors are with the Erik Johnsson School of Engineering and Computer Science, The University of Texas at Dallas, Richardson, TX 75080 USA (e-mail: mmahdavi@utdallas.edu; reza.moheimani@utdallas.edu).

Digital Object Identifier 10.1109/JSEN.2021.3052855

overall system. An alternative approach is to shape electrodes of the piezoelectric transducer to minimize the effect of resonances that lie outside of the controlled bandwidth. This technique is known as spatial filtering [16] or modal actuation/sensing [13].

Modal actuation and sensing utilize the orthogonality property of the structural mode shapes. In addition to macroscale flexible structures [13], [17], this technique has recently been implemented in MEMS devices [18], [19]. In these works, numerical and finite element models were developed to determine optimal placement and shape of electrodes on the piezoelectric sensors and actuators. In a MEMS resonator, optimal placement of electrodes can provide more efficient actuation of a specific resonance mode, while suppressing spurious modes in the frequency response of the resonator [18]. Similarly, electrodes on sensors or actuators of a microcantilever are shaped for operation at a specific resonance mode [19].

Here, we implement modal sensing/actuation on microcantilevers with two-layer stack piezoelectric transducers. By collocating two separate piezoelectric layers as actuation and sensing transducers, we are able to implement modal shaping as needed, thanks to the existing micromachining techniques. While the bottom transducer in this configuration is rectangular shaped, i.e., following the profile of the cantilever, the top transducer and the top electrode are shaped for modal actuation and sensing of the piezoelectric cantilever at the first flexural mode. Due to fabrication tolerances, higher modes still appear in the frequency response of the cantilever, but their magnitudes are small relative to the first mode. We use a time delay feedback controller to reduce Qs of these cantilevers. While spillover causes instability of the closed-loop system for a cantilever with both a rectangular actuator and sensor, the closed-loop system stays stable for a cantilever with a shaped transducer.

In this paper, we first develop a mathematical formulation of the modal transverse vibration of the structures studied here. Section III describes the microcantilever design and the microfabrication process used. In Section IV, experimental results are reported, including characterization of the piezoelectric actuator and sensor responses. In Section V, we discuss how spillover effect can be avoided by shaping the actuator or sensor. Finally, the paper is concluded in Section VI.

II. Actuation and Sensing of Modal Transverse Vibrations With Piezoelectric Transducers

Free transverse vibrations of a cantilever obeying Euler-Bernoulli beam theory, i.e., undergoing pure bending about y-axis are modeled by solving the partial differential equation:

$$C\frac{\partial^4\zeta(x,t)}{\partial x^4}+\mu\frac{\partial^2\zeta(x,t)}{\partial t^2}+r_a\frac{\partial\zeta(x,t)}{\partial t}=f(x,t), \quad (1)$$

where $\zeta(x,t)$ is the spatio-temporal vibration of the neutral axis, C, μ, and r_a are the flexural rigidity, the linear mass density of the beam along x-axis and the damping ratio, and $f(x,t)$ is the perpendicular applied force along the length of the cantilever. It is convenient to solve (1) as a homogeneous equation for undamped free vibrations, i.e., $f(x,t)=0$ and $r_a=0$. By separating independent time and space solutions, the result is a superposition of modal free vibrations:

$$\zeta(x,t)=\sum_{m=1}^{\infty}X_m(x)\phi_m(t), \quad (2)$$

where $X_m(x)$ is m^{th} free vibration mode shape (eigenfunction) and ϕ_m is the time-dependent magnitude of the m^{th} mode. Mode shapes of the cantilever beam are spatial solutions of (2) found by applying fixed and free vibration boundary conditions to the end and tip of the cantilever, respectively. The solution for the m^{th} mode shape can be expressed as:

$$X_m(x)=\left(\cosh k_ml(\frac{x}{l})-\cos k_ml(\frac{x}{l})\right) -\gamma_m\left(\sinh k_ml(\frac{x}{l})-\sin k_ml(\frac{x}{l})\right), \quad (3)$$

where k_ml represents the corresponding eigenvalue of the m^{th} mode. Table I includes first five eigenvalues k_ml and coefficients γ_m for the mode shape of (3).

TABLE I
EIGENVALUES AND AMPLITUDE RATIO COEFFICIENTS

m	1	2	3	4	5
k_ml	1.8751	4.6940	7.8547	10.9955	14.1371
γ_m	0.7340	1.0187	0.9992	1	1

In order to derive the time-dependent amplitude of each vibration mode $\phi_m(t)$, we transform (2) from time to frequency domain by taking the Laplace transform, which results in:

$$Z(x,s)=\sum_{m=1}^{\infty}X_m(x)\Phi_m(s). \quad (4)$$

Then, we insert (4) into the Laplace transform of (1) and solve for $\Phi_m(s)$. Using orthogonality of eigenfunctions within the cantilever length, $x\in[0,l]$, we have the transfer function of vibration amplitude at the m^{th} mode as:

$$\Phi_m(s)=\frac{\beta_m(s)}{s^2+\frac{\omega_m}{Q_m}s+\omega_m^2}, \quad (5)$$

$$\beta_m(s)=\frac{4}{\mu l}\int_0^l F(x,s)X_m(x)dx, \quad (6)$$

where the quality factor Q_m and resonance frequency ω_m of the m^{th} mode are:

$$Q_m=\frac{\mu\omega_m}{r_a}\ ,\ \omega_m=\frac{(k_ml)^2}{l^2}\sqrt{\frac{C}{\mu}}. \quad (7)$$

In an active microcantilever, using piezoelectric self-actuation and sensing mechanism, a piezoelectric transducer applies a bending moment to produce vibrations. Using constitutive piezoelectric equations [20], the piezoelectric bending moment M_p generated by the voltage V applied to the piezoelectric layer is expressed as:

$$M_p(s)=\frac{Wd_{31}c_{11}}{2h}\left[h_o^2-h_u^2\right]V(s), \quad (8)$$

$$m_p=\frac{M_p(s)}{V(s)}, \quad (9)$$

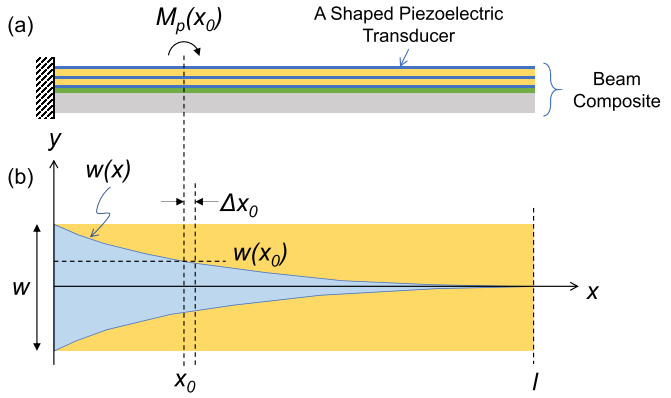

Fig. 1. (a) Beam composite under point piezoelectric moment $M_p(x_0)$ at distance x_0 from the anchor: Si cantilever, SiO_2 isolation layer, bottom electrode, bottom piezoelectric layer, middle electrode, top piezoelectric layer and top electrode from bottom to top. (b) Defining a differential element of piezoelectric bending moment for a cantilever with arbitrarily shaped top electrode on top of the piezoelectric actuator.

where W, h, d_{31}, and c_{11} are the width, thickness, transverse piezoelectric coefficient, and Young's modulus along the X axis, respectively. h_o and h_u are the distance of the bottom and top of the layer from the neutral axis of the composite beam. m_p is introduced here as a transduction factor, converting the voltage to the piezoelectric bending moment.

It is a common practice to model the presence of a concentrated force on the cantilever with a Dirac delta function, $\delta(x)$. Thus, the force generated by a concentrated point moment is presented as the first derivative of the delta function, $d\delta(x)/dx$ [17]. Using this convention and assuming a uniform surface coverage of the actuator along the cantilever length, we can define the force in (6) as [20]:

$$F(x,s) = M_p(s)\left[\frac{d\delta}{dx}(x-l) - \frac{d\delta}{dx}(x)\right]. \tag{10}$$

Therefore, the transfer function of transverse vibration along the length of the cantilever over the applied voltage becomes:

$$\frac{Z(x,s)}{V(s)} = -\frac{4m_p}{\mu l}\sum_{m=1}^{\infty}\frac{dX_m(l)}{dx}\frac{X_m(x)}{s^2+\frac{\omega_m}{Q}s+\omega_m^2}. \tag{11}$$

This equation is used to estimate the motion at the cantilever tip shown in Fig. 1. The beam composite consists of a 5 μm Si, 500 nm of SiO_2, 200 nm of Mo, 1 μm of AlN, 200 nm of Mo, 1 μm of AlN and 1 μm of Al layers from the bottom to the top. The cantilever length and width are respectively 354 μm and 100 μm. The frequency response function (FRF) of the displacement at the cantilever tip is numerically calculated and plotted in Fig. 2 with a dashed blue line over a wide frequency range to cover the first five resonance modes.

Eigenvalues and amplitude ratio coefficients listed in Table I are used to determine mode shapes and calculate their derivative. For x-coordinate, the cantilever length is divided into 1000 sections. Quality factors of 330, 545, 600, 300 and 200 are respectively used for 1st to 5th mode shapes. These values match our experimental results. Frequency responses are calculated at 10,000 points along the frequency axis. Simulations are performed in MATLAB, with long format precision, to ensure numerical accuracy of our calculations.

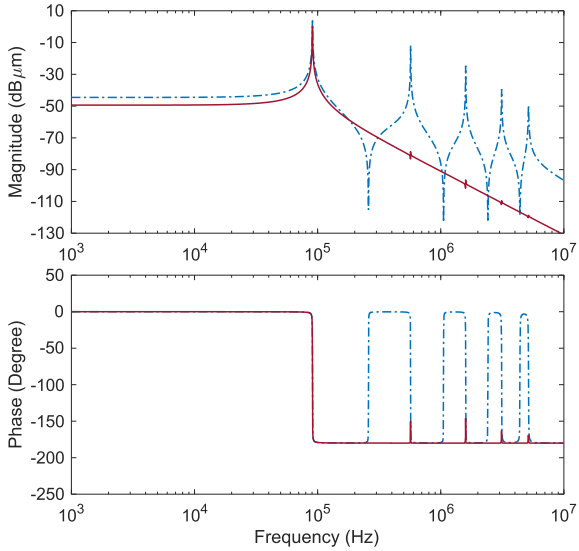

Fig. 2. Frequency response functions of the tip displacement over the actuation voltage for cantilevers with a rectangular shape and a shaped actuator, plotted in dashed blue and solid red lines, respectively.

A. Modal Actuator

Now, assume that the piezoelectric moment is produced by a transducer within a narrow area of width Δx_0 at a distance x_0 from the anchor point, and the electrode length has an arbitrary distribution of $w(x)$ along the cantilever length (see Fig. 1 (b)). The force created by this moment M_p is formulated as:

$$\Delta F(x,s) = M_p(x_0,s)\left[\frac{d\delta}{dx}(x-x_0) - \frac{d\delta}{dx}(x-x_0-\Delta x_0)\right]. \tag{12}$$

We repalce $M_p(s)$ with $M_p(x,s)$ to reflect coordinate dependency of the piezoelectric moment. Then, we can define the differential force applied along the cantilever length due to the concentrated moment at distance x_0 as:

$$dF(x,s) = M_p(x_0,s)\left[\frac{d^2\delta}{dx^2}(x-x_0)dx_0\right]. \tag{13}$$

By integrating (13) along the cantilever length, the total force is found as:

$$\begin{aligned} F(x,s) &= \int_{x_0=0}^{x} dF(x,s) \\ &= \int_{x_0=0}^{x} M_p(x_0,s)\left[\frac{d^2\delta}{dx^2}(x-x_0)dx_0\right] \\ &= \frac{d^2M_p(x,s)}{dx^2}. \end{aligned} \tag{14}$$

Incorporating (8) and (9) into this equation, we obtain:

$$F(x,s) = \frac{2m_pV(s)}{W}\frac{d^2w(x)}{dx^2}, \tag{15}$$

Note that $w(x)$ is the half electrode width. Therefore, it is divided by $W/2$ for correct electrode width normalization in (15).

$$\beta_m(s) = \frac{8m_p}{\mu l W}V(s)\int_0^l \frac{d^2w(x)}{dx^2}X_m(x)dx, \tag{16}$$

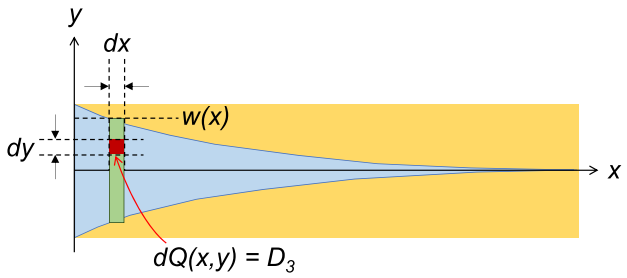

Fig. 3. Defining a differential element of stress-induced piezoelectric charge.

which means that time-dependent vibration amplitude at each mode is dependent on the second derivative of the electrode width distribution along the cantilever length. Then, orthogonality of the mode shapes along the cantilever length is used for spatial mode filtering. Shaping the piezoelectric actuator transducer or the electrode on the transducer corresponding to a specific mode shape is also known as modal actuation. To eliminate all the modes except the first, the electrode width distribution is designed as the second derivative of the mode shape at this mode, i.e.:

$$w(x) = \frac{W}{2}\frac{1}{k_1^2}\frac{d^2X_1(x)}{dx^2}. \tag{17}$$

Using (5) and (6), the frequency dependent vibration amplitude becomes:

$$\frac{Z(x,s)}{V(s)} = -\frac{m_p}{\mu}k_1^2\frac{X_1(x)}{s^2+\frac{\omega_1}{Q_1}s+\omega_1^2}. \tag{18}$$

Solid red line curve in Fig. 2 shows the FRF of the tip displacement over actuation voltage for a cantilever with a shaped actuator. The response is compared with FRF of the regular cantilever plotted with dashed blue line. We observe that all modes are eliminated from the frequency response of the tip displacement, except the first mode.

B. Modal Sensor

In a similar manner, shaping the piezoelectric transducer can be realized for modal sensing of cantilever vibration at a specific mode. The output charge of the sensor is an integration of piezoelectrically induced charges on differential surface area (see Fig. 3), and can be formulated as:

$$Q_p = \iint dQ(x,y)\,dxdy = \iint D_3(x,y)\,dxdy. \tag{19}$$

Using piezoelectric constitutive relations, we can replace the charge displacement D_3:

$$Q_p(s) = \int_0^l -\frac{2m_p}{W}\,w(x)\,\frac{d^2Z(x,s)}{dx^2}\,dx. \tag{20}$$

For a cantilever with a uniform surface coverage of the sensor, we will have:

$$\frac{Q_p(s)}{V(s)} = \frac{4m_p^2}{\mu l}\sum_{m=1}^{\infty}\left(\frac{dX_m(l)}{dx}\right)^2\frac{1}{s^2+\frac{\omega_m}{Q_m}s+\omega_m^2}. \tag{21}$$

The input/output voltage transfer function is derived as:

$$\frac{V_{out}}{V_{act}} = C_p\frac{Q_p(s)}{V_{act}(s)}, \tag{22}$$

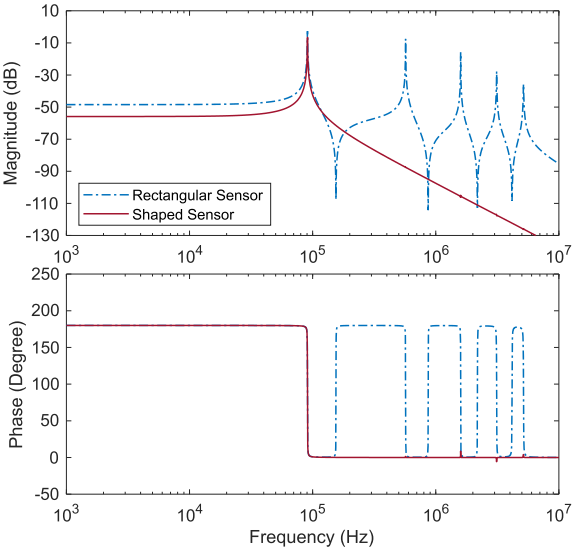

Fig. 4. Input/output transfer functions of the microcantilever's model. The dashed blue line is FRF of the cantilever with both the rectangular top and bottom transducers. The solid red line is FRF of the cantilever with the bottom rectangular actuator and the top shaped sense transducer for modal sensing of the 1st resonance mode.

where C_p is the electrical capacitance of the sense piezoelectric transducer. The transfer function for the cantilever with a rectangular shape actuator and sensor is numerically calculated and plotted with a dashed blue line in Fig. 4.

Now consider replacing $w(x)$ in (20) with the distributed electrode described in (17). Due to orthogonality of the eigenfunctions of the cantilever, all other mode shapes except the 1st mode will be eliminated from the output charge. Thus, the transfer function of output charge over input voltage can be described as:

$$\frac{Q_p(s)}{V(s)} = \frac{3.132m_p^2}{\mu}\frac{\int_0^l\left(\frac{d^2X_1(x)}{dx^2}\right)^2dx}{s^2+\frac{\omega_1}{Q_1}s+\omega_1^2}. \tag{23}$$

Input/output voltage transfer function of the cantilever with a modal sensor is plotted with solid red line in Fig. 4 for comparison.

In this section, we demonstrated how orthogonality of mode shapes of cantilever transverse vibrations can be used for modal actuation and sensing. The piezoelectric transducer is designed to selectively actuate or measure vibration at a specific resonance mode. This technique can be equivalently applied by shaping the actuator or sensor transducers, or by shaping the electrodes on the actuator or sensor. In either case, the distribution of the width of transducer/electrode along the cantilever length should be proportional to the 2nd derivative of the intended mode shape. Therefore, modal actuation and sensing are in fact reciprocal properties. Either method can be used to eliminate all mode shapes except for the desired mode. While the above equations are used for modal actuation/sensing of the first mode, they can be used for modal actuation/sensing of other mode shapes, as well. However, practical concerns such as microfabrication limits should be considered in realization of these approaches at higher resonance modes.

III. Design and Microfabrication

Modal actuation/sensing have been used by other researchers to shape piezoelectric patches of PVDF or PZT, attached to the macroscale flexible structures [13], [21]. As mentioned earlier, realization of these techniques at microscale, however, relies on microfabrication techniques. Thin film layers of piezoelectric transducers and metal electrodes are deposited, and are accordingly shaped with high precision photo-lithography, layer deposition and etching techniques.

We implement modal actuation/sensing on microcantilevers with a two-layer piezoelectric transducer. The structure is similar to that introduced in [22]: the two layer transducer is composed of a bottom electrode, a bottom piezoelectric layer, a middle electrode, a top piezoelectric layer, and a top electrode made of Mo, AlN, Mo, AlN and Al materials, from the bottom to the top. The whole stack is microfabricated on a Si microcantilever. The cantilever has a length of 345 μm and width of 100 μm. The top transducer is composed of the top AlN layer in-between the top and middle electrodes, while the bottom transducer is made of the bottom AlN layer in-between the middle and bottom electrodes. One of the two separate top and bottom transducers is utilized to excite the cantilever vibration, while the other is used for reading out the cantilever deflection.

These microcantilevers are designed for atomic force microscopy. A feedback control loop can be used to reduce their quality factor as required. Modal actuation and sensing improve stability robustness of these feedback loops.

A. Microfabrication

A process is developed for microfabrication of these cantilevers. Different steps of the device fabrication are discussed in detail later in this section. The scanning electron microscopy (SEM) images of cantilevers are shown in Fig. 5. Two types of microcantilevers are designed and fabricated. In the first design both the bottom and top transducers are rectangular shape as shown in Fig. 5(a). In the second design, the top transducer is shaped for modal actuation or sensing at the 1st flexural resonance mode, while the bottom transducer is rectangular (See Fig. 5(b)).

Microfabrication of the cantilevers is done on a 4" p-type doped silicon-on-insulator (SOI) wafer, type <100> with 400 μm thick handling layer, 1 μm thick buried oxide and 5 μm thick silicon device layers. The fabrication process starts with growing a 500 nm thick thermal oxide layer between the silicon substrate and the bottom electrode (Fig 5. (a)). In the next step, a stack of four layers of Mo/AlN/Mo/AlN with thicknesses of 200 nm/1000 nm/200 nm/1000 nm is sputtered on the wafer (Fig. 6(b)). The Mo layers act as the middle and the bottom electrodes, and the AlN layers act as the top and the bottom piezoelectric transducers, respectively. Prior to each of AlN/Mo layer photolithography step, a 200 nm oxide layer is deposited by Plasma Enhanced Chemical Vapor Deposition (PECVD) as a sacrificial mask layer which is stripped by BOE after each AlN/Mo etch process.

The first photolithography step is done to pattern and etch the top AlN layer (Fig. 6(c)). Etching of AlN is done by

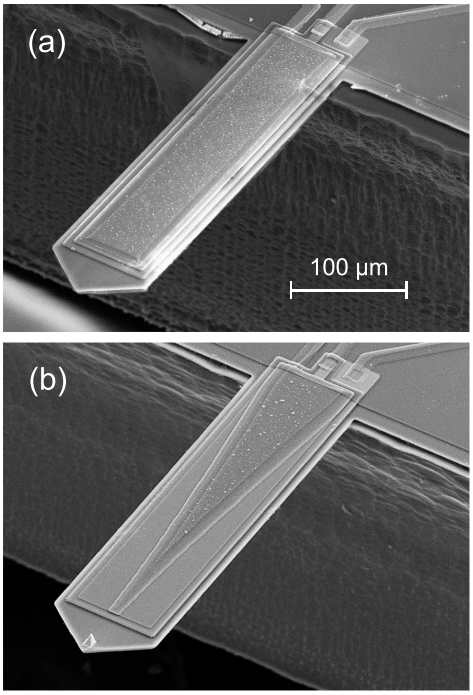

Fig. 5. SEM images of the microfabricated cantilevers with a two-layer stack transducer. (a) Both the top and bottom transducers are rectangular. (b) The bottom transducer is rectangular, but the top transducer is shaped for modal actuation/sensing at the 1st mode.

Reactive Ion Etching (RIE) of oxide layer with CHF3/Ar plasma and the AlN with chlorine-based plasma. A wet etch process is used to remove the possible residues of the AlN layer with 2.5% TMAH solution at 80° C. In the next step, the middle Mo layer, is patterned and etched by chlorine-based plasma (Fig. 6(d)) and is followed by a similar patterning and etching of AlN/Mo layers as the bottom piezoelectric and bottom electrodes, respectively (Fig. 6(e),(f)). Then, a 500 nm PECVD silicon oxide layer is deposited on the wafer as the electrical isolation layer between metal electrodes. This layer is patterned and etched by CHF3/Ar plasma in RIE tool for providing access to the middle and bottom electrodes (Fig. 6(g)). In the next step, 1 μm thick aluminum layer is deposited by an electron beam evaporation tool and is lifted-off to pattern the contact pads of the cantilevers (Fig. 6(h)). Cantilever bodies are patterned in the following step by etching the 5 μm silicon device layer with DRIE tool (Fig. 6(i)). Backside silicon etch is performed by a Bosch process in a DRIE tool. To protect the features on the front side of the wafer, a 1 μm thick Parylene protection layer is deposited on the SOI top surface. By completing the backside silicon etching, the 1 μm thick box layer is etched to release the cantilevers completely (Fig. 6(j)). Figure 6(k) shows the schematic of the cantilever body with shaped top AlN layer, modeled in CoventorWare software. After cleaning the cantilevers in oxygen plasma, the nanoscale sharp platinum tips are fabricated using a FEI Nova 200 focused ion beam (FIB).

IV. Experimental Results

Characterization of the microfabricated cantilevers are reported in this section. The experiments are conducted on three separate cantilevers. The first is a conventional active

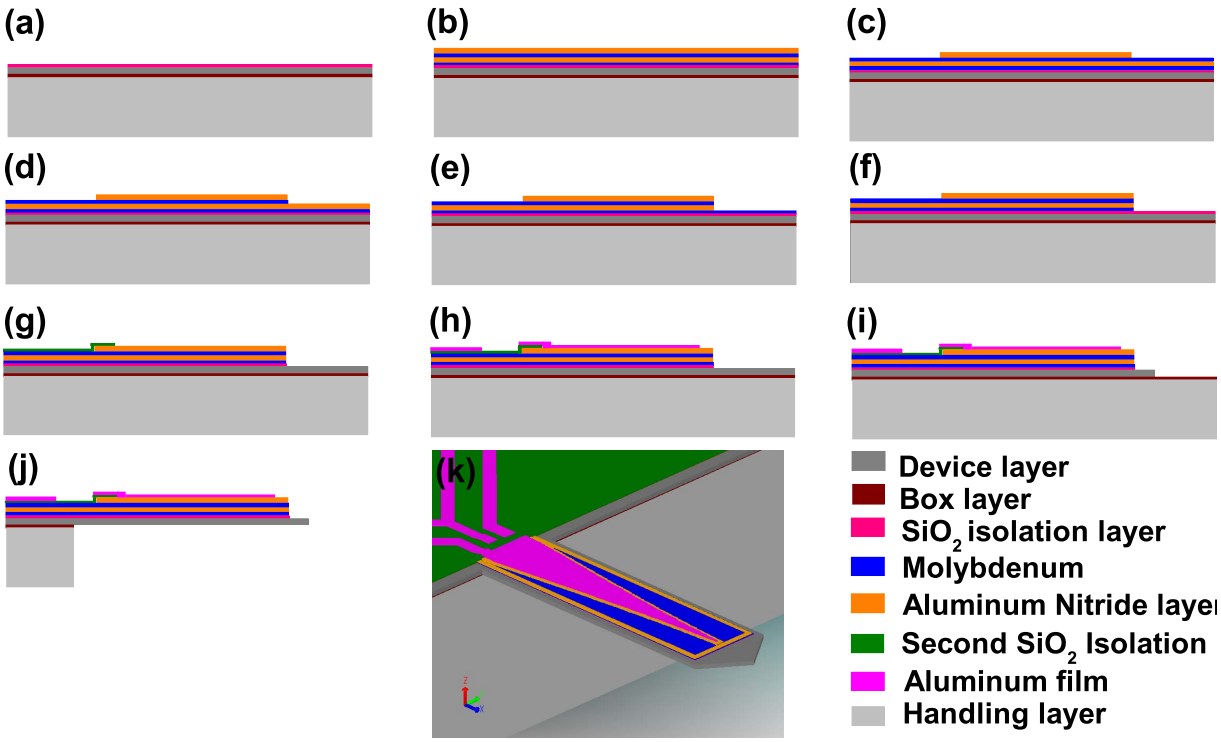

Fig. 6. SEM images of the microfabricated cantilevers with a two-layer stack transducer. (a) Thermal oxide growth, (b) stack deposition of Mo/AlN/Mo/Al layers, (c) Shaping the top piezoelectric transducer, (d) Shaping the middle electrode, (e) Shaping the bottom piezoelectric transducer, (f) Shaping the bottom electrode, (g) Second oxide isolation deposition and etching, (h) Lifting-off the top electrode, (i) Shaping microcantilevers, (j) Releasing the microcantilevers and (k) A final microfabricated cantilever.

cantilever with rectangular actuator and sensor transducers. The second cantilever has a modal sensor, which is actuated with a rectangular bottom transducer, and a shaped top transducer as a sensor. The third set of experiments are performed with a similar cantilever, but the top shaped transducer is used for actuation and the bottom rectangular transducer for sensing.

A. Actuator Characterization

We first study the effect of modal actuation on the microfabricated cantilevers' transverse vibrations. A periodic chirp signal with an amplitude of 100 mV is applied to the piezoelectric actuator. The displacement of the cantilevers' tip is measured using a laser Doppler vibrometer (LDV), Polytech MSA-100 instrument. FRFs of the tip displacements of these three cantilevers are plotted in Fig. 7. The dashed blue line shows FRF of the cantilever with a rectangular actuator and sensor. The red and green lines belong to cantilevers with a shaped top transducer and a bottom rectangular transducer. The bottom and the top transducers are actuated respectively in red and green graphs.

When the cantilever is excited with a rectangular bottom or top transducer (red and blue), 2nd and 3rd modes are visibly excited as we would expect from (11). Indeed all resonance modes are expected to appear in the frequency response of the cantilever. On the contrary, if the top shaped transducer is used for cantilever excitation, one would expect elimination of the higher modes according to (18). However, for the microfabricated cantilevers studied here, higher resonance modes do

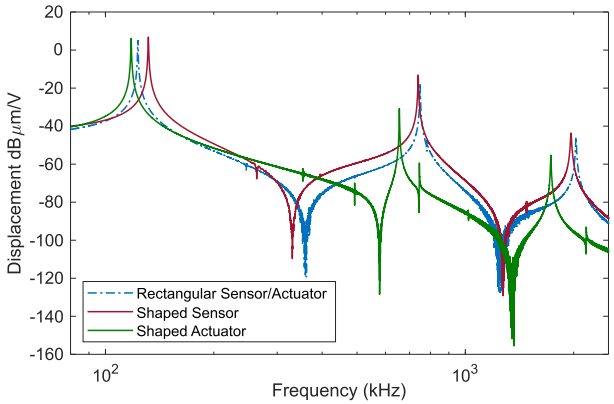

Fig. 7. Frequency responses of cantilevers displacement acquired with an LDV: dashed blue, red solid and green solid lines belong to microcantilevers with rectangular actuator/sensor, rectangular actuator/shaped sensor and shaped actuator/rectangular sensor, respectively.

appear in FRF, but their amplitudes are more than an order of magnitude smaller.

The actuation gains of the three cantilevers are summarized in Table II at the 1st and 2nd resonance modes. Due to modal actuation, the gain of 2nd mode is smaller in the shaped actuator in comparison with those cantilevers with rectangular actuators.

Two major factors can be identified as root-causes of deviation of responses from the ideal model presented in Section II. First, the cantilevers geometry is no longer rectangular. Therefore, mode shapes of the presented cantilevers are slightly different from the rectangular cantilevers. Using a picket shape

TABLE II
ACTUATION AND SENSE PERFORMANCE

Mode	Actuator Gain μm/V 1st	Actuator Gain μm/V 2nd	Sensor Gain V/μm 1st	Sensor Gain V/μm 2nd	Coupling Factor k_d^2 1st	Coupling Factor k_d^2 2nd
Rectangular Actuator/Sensor	1.53	0.14	1.12	10.42	6.64	1.3%
Shaped Sensor	1.62	0.22	1.22	0.29	9.85	0.56%
Shaped Actuator	2.12	0.01	2.09	23.7	14.1	0.55%

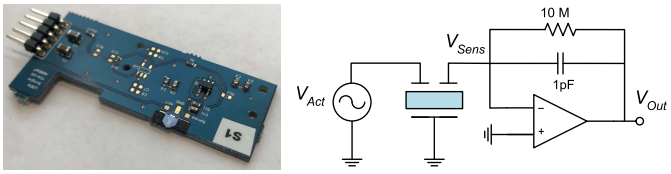

Fig. 8. Image of the printed circuit board (PCB) and schematic of the charge amplifier circuit.

cantilever is inevitable for our studies. A Pt tip is deposited at the end of the cantilever and used in AFM experiments. To avoid possible electrical shorts during Pt deposition in FIB, we had to allow enough room between transducers and the tip. Therefore, the cantilever had to be elongated and tapered at the end. This additional part results in a slight difference between analytical models and experimental results. The added mass of the Pt tip will further change the cantilever dynamics. We chose a triangular shaped extension since it has the least effect on the cantilever dynamics. The effect of the extra part becomes more important at higher modes where dimensions of the extension become more comparable with the wavelength of those modes. Second, since the transducer and electrodes do not extend all the way to the end, implementation of an ideal second derivative of the first mode shape is not possible. The resulting difference between the shape of the electrode and the mode shape derivative causes residuals in integral of (23).

B. Sensor Output Response

In Section II, we calculated the relationship between a cantilever's deflection and induced charges on its piezoelectric sensor. Using a charge amplifier readout circuit (see Fig. 8), the sensor output charge is amplified and converted to a voltage. To acquire input/output transfer functions of the microcantilevers a lock-in amplifier (LIA), Zurich Instrument HF2LI, is used. A sine voltage with an amplitude of 100 mV is applied to the actuator. The sense transducer's electrode is connected to the charge amplifier. The input/output FRFs are plotted and compared in Fig. 9. Resonant responses of the cantilever at the 1st, 2nd and 3rd modes are shown in (a), (b) and (c), respectively.

The dashed blue lines show the response of the micro-cantilever with rectangular actuator and sensor. The solid red lines show the sensor outputs for the cantilever with a shaped (top) actuator and a rectangular (bottom) sensor. The solid green lines plot the response for a similar cantilever on which actuator and sensor are swapped. Deflection sensing gains are also extracted and summarized in Table II. From the plots and deflection sensitivities, we observe that still the 2nd and 3rd modes appear in frequency responses of both cantilevers with a shaped actuator and sensor.

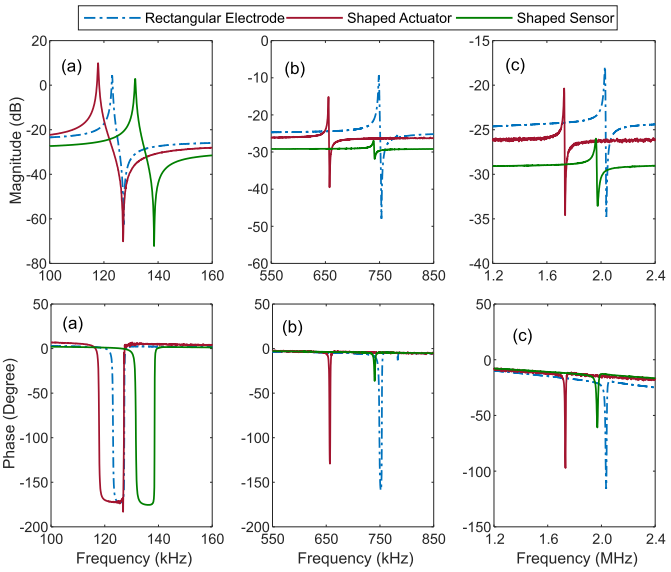

Fig. 9. Sensor outputs comparison: (a) 1st, (b) 2nd and (c) 3rd resonance modes. Dashed blue lines, solid red lines and solid green lines show FRFs of cantilevers with rectangular/rectangular, shaped/rectangular and rectangular/shaped actuator/sensor, respectively.

However, the output voltage/charge is relatively smaller than the one with both rectangular actuator and sensor.

To have a quantitative insight of reciprocity of modal actuation and sensing, we employ piezoelectric electromechanical coupling coefficients k_d^2 at the first two resonance modes. The electromechanical coupling coefficient is a measure of energy transduction efficiency from electrical to mechanical domain and vice versa. These coefficients are calculated for each mode based on Mason's relation, defined as [23]:

$$k_d^2 = \frac{\omega_a^2 - \omega_r^2}{\omega_a^2} \tag{24}$$

in which, ω_r is the resonance frequency of each mode and ω_a^2 is the closest anti-resonance or zero to the resonance frequency. These coefficients are also calculated and summarized in Table II. From these coefficients, we may conclude that modal actuation and sensing result in higher electromechanical coupling at the 1st mode and lower coupling at other modes, compared with a cantilever with a rectangular actuator and sensor.

Sensor output response together with deflection response, acquired with LDV, for the cantilever with a rectangular actuator and a shaped sensor is plotted in Fig. 10. Since the cantilever is excited with a rectangular actuator, higher resonance modes appear in the deflection response (see dashed blue line). The sensor output (solid red line) follows the cantilever dynamics, especially around the first intended resonance mode. Out of resonance sensor output response, however, slightly deviates from the deflection response, due to a small feedthrough capacitance between the actuation and sense ports. The 2nd and 3rd modal responses are heavily submerged in the feedthrough.

The presence of higher order modes in modal sensor response can be explained in a similar manner. In the next section we demonstrate that despite these deviations, modal

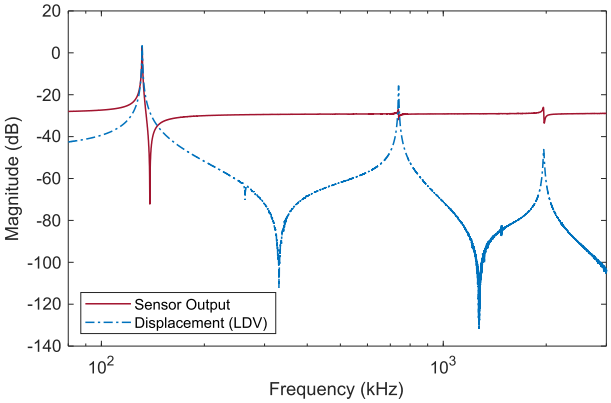

Fig. 10. Comparing deflection response with sensor output response of the cantilever with a rectangular actuator and a shaped sensor.

actuation and sensing have important implications on closed loop stability of a Q-controlled cantilever.

V. Q Control

In tapping mode atomic force microscopy, it is sometimes desirable to increase the Q-factor of a cantilever. First, higher Q-factors result in a higher force sensitivity, which provides a better resolution during imaging. Second, while imaging in a liquid environment, viscous losses significantly reduce the cantilever's Q, therefore reducing its force sensitivity. In this case, it is similarly desirable to increase the Q-factor to increase the force sensitivity. Furthermore, the force exerted between the probe tip and the sample F_{TS} is inversely proportional to the cantilever's Q; meaning that to minimize deformation of a soft sample, it is preferable to increase the Q-factor [24].

On the contrary, lowering a cantilever's Q-factor is necessary to increase the imaging speed and avoiding probe loss in a high-speed tapping-mode AFM [25]. Probe loss occurs on steep downward steps at which the cantilever amplitude changes cannot follow the rapid changes of the topography. Instead, the cantilever vibration amplitude, $z(t)$, changes according to the following equation [26]:

$$z(t) = z_{set} + (z_0 - z_{set})(1 - e^{-\frac{\omega_n}{2Q}t}). \tag{25}$$

where z_{set}, z_0 and ω_n are set, free vibration amplitudes and resonance frequency of the cantilever, respectively. The vibration amplitude increases up to z_0 and saturates at this amplitude, until it lands back on the sample. This effect is known as parachuting [27].

Also, slow transient response of the cantilever, predominantly, slows down the transient response of the AFM z-axis. In this case, Q is decreased to allow z-axis controller gain to be increased. This results in a wider closed-loop bandwidth for increasing the scanning speed [26].

A. Active Q Control

Active control of the cantilever's Q-factor is performed by implementing a feedback loop that uses the deflection signal. A simple implementation, but commonly used method, is the time delay Q control [28]. A simplified differential equation describes the deflection of the cantilever's tip when the AFM

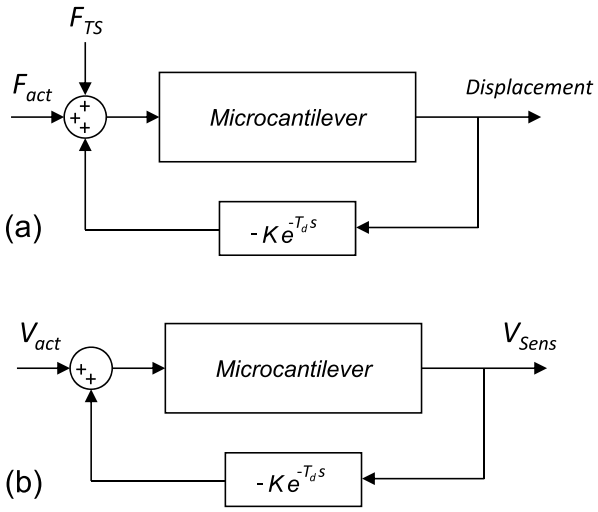

Fig. 11. (a) Block diagram of cantilever's active Q control using time delay method. (b) Implementation of a closed-loop system for active Q control of the cantilever with an integrated sensor and actuator.

is operating in tapping mode [28]:

$$mz''(t) + \frac{m\omega_n}{Q}z'(t) + kz(t) = A_0\cos(\omega t) + F_{TS}(t). \tag{26}$$

in which m, k and $z(t)$ are the effective mass, the stiffness and tip transverse vibration of the cantilever. Two forces are acting on the cantilever: 1) the force induced by piezoelectric actuation with amplitude of A_0 at frequency ω and 2) the force due to tip-sample interaction $F_{TS}(t)$. Now, if we add a force proportional to tip velocity to the right hand side of the equation, the effective Q can be modified [28]:

$$mz''(t)+\frac{m\omega_n}{Q}z'(t)+kz(t)=A_0\cos(\omega t)+F_{TS}(t)-Gz'(t). \tag{27}$$

The block diagram of an active Q control using delay method is shown in Fig. 11(a). To implement this method on microcantilevers with an integrated sensor and actuator, the sensor output V_{sens} is delayed by a time period T_d $(= 1/4f_0)$ that corresponds to a $-90°$ phase shift at resonance. The delayed signal, proportional to the tip velocity, is multiplied by gain K to be added to the cantilever's actuation signal V_{act} (see Fig. 11(b)). The gain K determines the level of Q-factor modification, while its polarity determines if the feedback loop results in an enhanced or a reduced Q-factor.

To theoretically modify Q-factor of the cantilevers under this study at the 1st resonance mode, we design and implement closed-loop systems in MATLAB. FRFs of cantilevers acquired by LIA are used as open loop systems. Open loop responses of cantilevers with a rectangular/rectangular and shaped/rectangular actuator/sensor are plotted in Fig. 12(a) and (c), respectively. While modeling the cantilever to control Q at the 1st mode, unmodeled higher modes are excited by control action. This phenomenon is known as the spillover effect, and can bring the closed-loop system into instability [14], [29].

Initially, delay Q control method is used to reduce Q-factor of the cantilever with both rectangular actuator and sensor from 362 to 30. It is evident in Fig. 12(a) and (b), while Q at

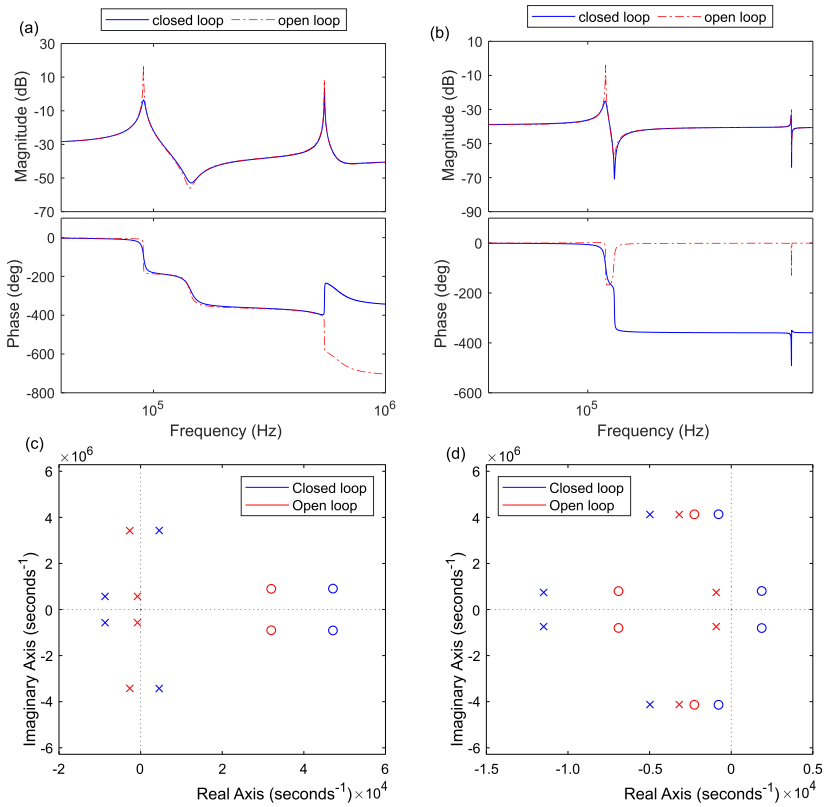

Fig. 12. (a) and (c) Active Q control of cantilevers with rectangular/rectangular and shaped/rectangular piezoelectric actuator/sensor using delay method. (b) and (d) Zero-pole maps of the same cantilevers before and after Q control.

the first mode is modified poles of the second mode are moved to the right hand side of the $j\omega$ axis and the closed-loop system becomes unstable.

We use the same method to modify Q of cantilever with a modal actuator and a rectangular sensor. It is shown that spillover, seen in the cantilever with rectangular actuator/sensor, can be eliminated by modal actuation/sensing of the cantilever.

From Fig. 12(c) and (d), it is visible that the poles of the second mode of the cantilever stay stable, while Q of the cantilever with modal actuator is reduced to 30. Contrary to the cantilever with rectangular actuator and sensor, poles of the second mode are moved further away toward left hand side of the $j\omega$ axis; therefore the closed-loop stays stable even at higher feedback gains.

VI. Conclusion

In this work, we reported implementation of modal actuation and sensing on AFM microcantilevers with a two-layer stack transducer. While the top transducer in the stack is shaped to follow 2nd derivative of the cantilever mode shape at the 1st resonance mode along its length, the bottom transducer is uniformly distributed along the cantilever length. We demonstrated that spatial filtering or modal actuation/sensing can eliminate higher resonance modes of the cantilever. When the cantilever is used in a closed-loop system, the system does not experience the spillover effect and stays stable. On the contrary, the cantilever without modal actuator/sensor becomes unstable when its Q is reduced at the same rate.

Acknowledgment and Disclaimer

The authors would like to thank cleanroom staff at The University of Texas at Dallas.

References

[1] D. E. Serrano *et al.*, "Substrate-decoupled, bulk-acoustic wave gyroscopes: Design and evaluation of next-generation environmentally robust devices," *Microsyst. Nanoeng.*, vol. 2, no. 1, p. 16015, Dec. 2016.

[2] A. G. Fowler, A. N. Laskovski, A. C. Hammond, and S. O. R. Moheimani, "A 2-DOF electrostatically actuated MEMS nanopositioner for on-chip AFM," *J. Microelectromech. Syst.*, vol. 21, no. 4, pp. 771–773, Aug. 2012.

[3] M. Maroufi, A. Bazaei, and S. O. Reza Moheimani, "A high-bandwidth MEMS nanopositioner for on-chip AFM: Design, characterization, and control," *IEEE Trans. Control Syst. Technol.*, vol. 23, no. 2, pp. 504–512, Mar. 2015.

[4] F. Beyeler *et al.*, "Monolithically fabricated microgripper with integrated force sensor for manipulating microobjects and biological cells aligned in an ultrasonic field," *J. Microelectromech. Syst.*, vol. 16, no. 1, pp. 7–15, Feb. 2007.

[5] M. Maroufi, H. Alemansour, M. B. Coskun, and S. O. R. Moheimani, "An adjustable-stiffness MEMS force sensor: Design, characterization, and control," *Mechatronics*, vol. 56, pp. 198–210, Dec. 2018.

[6] A. Alipour, M. B. Coskun, and S. O. R. Moheimani, "A high bandwidth microelectromechanical system-based nanopositioner for scanning tunneling microscopy," *Rev. Sci. Instrum.*, vol. 90, no. 7, Jul. 2019, Art. no. 073706.

[7] S. C. Minne, S. R. Manalis, and C. F. Quate, "Parallel atomic force microscopy using cantilevers with integrated piezoresistive sensors and integrated piezoelectric actuators," *Appl. Phys. Lett.*, vol. 67, no. 26, pp. 3918–3920, Dec. 1995.

[8] S. R. Manalis, S. C. Minne, and C. F. Quate, "Atomic force microscopy for high speed imaging using cantilevers with an integrated actuator and sensor," *Appl. Phys. Lett.*, vol. 68, no. 6, pp. 871–873, Feb. 1996.

[9] S. S. Aphale, A. J. Fleming, and S. O. R. Moheimani, "Integral resonant control of collocated smart structures," *Smart Mater. Struct.*, vol. 16, no. 2, pp. 439–446, Feb. 2007.

[10] J. J. Dosch, D. J. Inman, and E. Garcia, "A self-sensing piezoelectric actuator for collocated control," *J. Intell. Mater. Syst. Struct.*, vol. 3, no. 1, pp. 166–185, Jan. 1992.
[11] U. Stöbener and L. Gaul, "Modal vibration control for PVDF coated plates," *J. Intell. Mater. Syst. Struct.*, vol. 11, no. 4, pp. 283–293, Apr. 2000.
[12] V. Sethi and G. Song, "Optimal vibration control of a model frame structure using piezoceramic sensors and actuators," *J. Vib. Control*, vol. 11, no. 5, pp. 671–684, May 2005.
[13] C.-K. Lee and F. C. Moon, "Modal sensors/actuators," *J. Appl. Mech.*, vol. 57, no. 2, pp. 434–441, Jun. 1990.
[14] J. Bontsema and R. F. Curtain, "A note on spillover and robustness for flexible systems," *IEEE Trans. Autom. Control*, vol. AC-33, no. 6, pp. 567–569, Jun. 1988.
[15] J. Qiu and M. Haraguchi, "Vibration control of a plate using a self-sensing piezoelectric actuator and an adaptive control approach," *J. Intell. Mater. Syst. Struct.*, vol. 17, nos. 8–9, pp. 661–669, Sep. 2006.
[16] A. Preumont, P. De Man, A. François, N. Loix, and K. Henrioulle, *Spatial Filtering With Discrete Array Sensors and Distributed PVDF Films*. Berlin, Germany: Springer, 2004, pp. 89–116.
[17] C. K. Lee, "Theory of laminated piezoelectric plates for the design of distributed sensors/actuators. Part I: Governing equations and reciprocal relationships," *J. Acoust. Soc. Amer.*, vol. 87, no. 3, pp. 1144–1158, Mar. 1990.
[18] J. Pulskamp *et al.*, "Electrode-shaping for the excitation and detection of permitted arbitrary modes in arbitrary geometries in piezoelectric resonators," *IEEE Trans. Ultrason., Ferroelectr., Freq. Control*, vol. 59, no. 5, pp. 1043–1060, May 2012.
[19] S. I. Moore, M. G. Ruppert, and Y. K. Yong, "Design and analysis of piezoelectric cantilevers with enhanced higher eigenmodes for atomic force microscopy," in *Proc. IEEE Int. Conf. Adv. Intell. Mechatronics (AIM)*, Jul. 2017, pp. 719–724.
[20] R. G. Ballas, *Piezoelectric Multilayer Beam Bending Actuators*. Berlin, Germany: Springer-Verlag, 2007.
[21] H. S. Tzou and J. J. Hollkamp, "Collocated independent modal control with self-sensing orthogonal piezoelectric actuators (theory and experiment)," *Smart Mater. Struct.*, vol. 3, no. 3, pp. 277–284, Sep. 1994.
[22] M. Mahdavi, M. B. Coskun, and S. O. R. Moheimani, "High dynamic range AFM cantilever with a collocated piezoelectric actuator-sensor pair," *J. Microelectromech. Syst.*, vol. 29, no. 2, pp. 260–267, Apr. 2020.
[23] S. H. Chang, N. N. Rogacheva, and C. C. Chou, "Analysis of methods for determining electromechanical coupling coefficients of piezoelectric elements," *IEEE Trans. Ultrason., Ferroelectr., Freq. Control*, vol. 42, no. 4, pp. 630–640, Jul. 1995.
[24] M. Fairbairn and S. O. R. Moheimani, "Sensorless enhancement of an atomic force microscope micro-cantilever quality factor using piezoelectric shunt control," *Rev. Sci. Instrum.*, vol. 84, no. 5, May 2013, Art. no. 053706.
[25] T. Sulchek *et al.*, "High-speed tapping mode imaging with active Q control for atomic force microscopy," *Appl. Phys. Lett.*, vol. 76, no. 11, pp. 1473–1475, 2000.
[26] T. Sulchek, G. G. Yaralioglu, C. F. Quate, and S. C. Minne, "Characterization and optimization of scan speed for tapping-mode atomic force microscopy," *Rev. Sci. Instrum.*, vol. 73, no. 8, pp. 2928–2936, Aug. 2002.
[27] M. B. Coskun, H. Alemansour, A. G. Fowler, M. Maroufi, and S. O. R. Moheimani, "Q control of an active AFM cantilever with differential sensing configuration," *IEEE Trans. Control Syst. Technol.*, vol. 27, no. 5, pp. 2271–2278, Sep. 2019.
[28] M. W. Fairbairn and S. O. R. Moheimani, "Control techniques for increasing the scan speed and minimizing image artifacts in tapping-mode atomic force microscopy: Toward video-rate nanoscale imaging," *IEEE Control Syst.*, vol. 33, no. 6, pp. 46–67, Dec. 2013.
[29] M. Balas, "Feedback control of flexible systems," *IEEE Trans. Autom. Control*, vol. AC-23, no. 4, pp. 673–679, Aug. 1978.